In vivo simultaneous multispectral fluorescence imaging with spectral multiplexed volume holographic imaging system

Yanlu Lv
Jiulou Zhang
Dong Zhang
Wenjuan Cai
Nanguang Chen
Jianwen Luo

In vivo simultaneous multispectral fluorescence imaging with spectral multiplexed volume holographic imaging system

Yanlu Lv,[a] Jiulou Zhang,[a] Dong Zhang,[a] Wenjuan Cai,[a] Nanguang Chen,[b] and Jianwen Luo[a,c,*]
[a]Tsinghua University, Department of Biomedical Engineering, Haidian District, Beijing 100084, China
[b]National University of Singapore, Department of Biomedical Engineering, Singapore 117576, Singapore
[c]Tsinghua University, Center for Biomedical Imaging Research, Haidian District, Beijing 100084, China

Abstract. A simultaneous multispectral fluorescence imaging system incorporating multiplexed volume holographic grating (VHG) is developed to acquire multispectral images of an object in one shot. With the multiplexed VHG, the imaging system can provide the distribution and spectral characteristics of multiple fluorophores in the scene. The implementation and performance of the simultaneous multispectral imaging system are presented. Further, the system's capability in simultaneously obtaining multispectral fluorescence measurements is demonstrated with *in vivo* experiments on a mouse. The demonstrated imaging system has the potential to obtain multispectral images fluorescence simultaneously. © *2016 Society of Photo-Optical Instrumentation Engineers (SPIE)* [DOI: 10.1117/1.JBO.21.6.060502]

Multispectral imaging is a technique that can simultaneously acquire spectral and positional information of the objects at several key wavelengths,[1] and it has been applied to the visualization of various superficially located diseases. Multispectral imaging can be achieved by acquiring individual band measurements with a filter wheel.[2] In order to study important transient scenes such as fast biochemical reactions and cellular dynamic events in a single piece of tissue, it is desirable to acquire multispectral images of biological tissues at high temporal resolution. Liquid crystal tunable filter[3] and acousto-optic tunable filter[4] have been used to increase the speed of spectral scanning. However, these filters are polarization sensitive and suffer from poor light throughputs.[5] In addition, the sequential

acquisition mode is the intrinsic barrier that cannot be easily overcome. Therefore, some video-rate hyperspectral imaging technologies such as multiple apertures,[6] reformatting,[7] and inversion[8] have been considered. However, these techniques require complex components, precise alignments and intensive computations. Beside, in many cases, the acquisition of the complete hyperspectral data cube provides little additional information compared with multispectral imaging, wherein images are acquired only in several discrete spectral bands.[9] Multiplexed volume holographic grating (VHG) has been employed for multidepth biomedical imaging applications to reduce the need of spatial scanning.[10,11] In the system, each hologram superimposed within the recording material is Bragg matched to a specific wave front that originates at a particular object plane located at different depths.

In this paper, a simultaneous multispectral imaging system using spectral multiplexed VHG is developed. Different from the aforementioned multidepth imaging systems, this system can simultaneously obtain both multiple spectral and positional information of fluorophores in the same object plane without wavelength scanning. A four-wavelength multiplexed VHG is used is this paper. Each hologram can selectively diffracts a target wavelength emitted from the same object plane using a designed reconstruction angle.[11,12] The multiplexed VHG (thickness 1.1 mm, clear aperture $7 \times 11 \text{ mm}^2$) contains four volume holograms designated for 620, 530, 488, and 590 nm, respectively. The nominal incident angle θ_{in} in air is 15 deg. To make full use of the effective area of the charged-coupled-device (CCD) detector (Andor Clara, 1392×1040 effective pixels) and avoid overlap among the laterally separated multispectral images, the separation angle $\Delta\theta$ between the diffracted beams is designed as 1.5 deg. In order to achieve high-quality imaging performance, this VHG is custom-designed and fabricated by OptiGrate Corp (Oviedo, Florida). The parameters of the multiplexed VHG are given in Table 1.

The reconstruction operation of the multiplexed VHG with multiple wavelength beams is shown in Fig. 1(a). For simplicity, the k-sphere diagram consisting of two grating vectors, $K_{g,1}$ for blue laser $\lambda_B = 488$ nm and $K_{g,2}$ for yellow laser $\lambda_Y = 590$ nm, is shown in Fig. 1(b). $k_{i,Y}$ and $k_{d,Y}$ are the wave vectors of the yellow incidence and diffraction beams, respectively. $k_{i,B}$ and $k_{d,B}$ are the wave vectors of the blue incidence and diffraction beams, respectively. The angle of the diffracted yellow beam is $\theta_{1,\text{dif}} = 13.5$ deg and the separation angle between the two diffracted beams is $\Delta\theta = 1.5$ deg.

Figure 2(a) shows the experimental setup for measuring the spectral-angular selectivity of the four holograms with separate monochromatic lasers.[13] The intensity of the incident light P_{inc} and diffracted light P_{dif} is measured by a power meter (Coherent LabMax-top). The diffraction intensity data are collected with the rotation step of 0.008 deg. Figure 2(b) shows the spectral-angular selectivity curve given by

$$\eta(\%) = P_{\text{dif}}/P_{\text{inc}} \times 100\%. \quad (1)$$

Figure 3 shows the experimental setup of the proposed system using the multiplexed VHG with four holograms. The imaging object is illuminated by a white light source (ASAHI SPECTRA MAX-302). The scattered light from the object is collected by the C-mount lens. Then, an intermediate image

*Address all correspondence to: Jianwen Luo, E-mail: luo_jianwen@tsinghua.edu.cn

Table 1 Parameters of the four multiplexed volume holograms.

Center wavelength (nm)	620	530	488	590
Grating period (μm)	1.091	0.976	0.943	1.198
Spectral-angular selectivity FWHM (deg)	0.0319	0.0311	0.0296	0.0376
Diffraction efficiency (%)	82.5	84.4	81.8	82.3

is formed on the plane of the rectangular aperture, colocated at the front focal plane of the collimating lens (Thorlabs AC254-100-A, focal length 100 mm). The multiplexed VHG is located at the Fourier plane of the $4f$ system, formed by the collimating lens and the collector lens (Thorlabs AC254-075-A, focal length 75 mm). When the multispectral imaging system is illuminated by its target wavelengths emitted from the object, images with different spectral characteristics are projected to different lateral locations on the CCD detector.

The images in Fig. 4(a) are taken in reflection mode with the Xenon lamp. The spatial resolution Δx of the whole system mainly depends on the focal length f_{col} of the collimating lens, the thickness L of the VHG[14] and the scaling M of the intermediate image created by the front-end C-mount lens [Eq. (2)].

$$\Delta x = \frac{1}{M} \frac{2\lambda f_{col}}{\theta_s L}, \quad (2)$$

where λ is the center wavelength of the probe beam, and θ_s is the angle between the incident beam and the diffracted beam. With
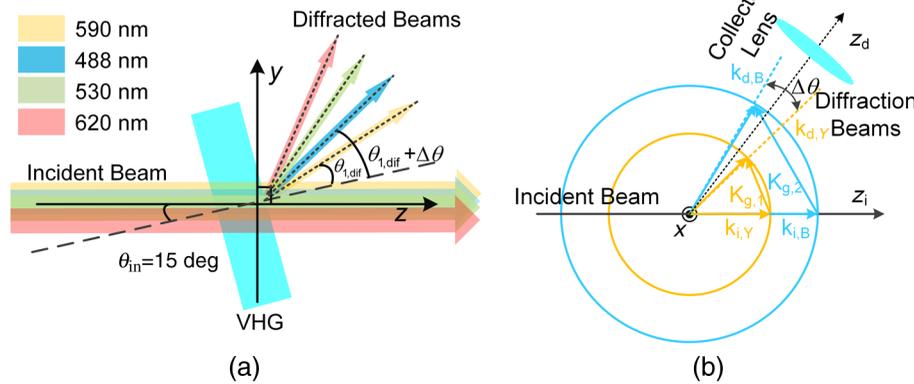
Fig. 1 Geometry of the reconstruction operation of the multiplexed VHG. (a) When the collimated beam containing four target wavelengths arrives at the VHG with an incident angle of $\theta_{in} = 15$ deg, the multiplexed VHG diffracts the corresponding Bragg-matched components into four different directions. (b) k-sphere diagram of probing the multiplexed VHG recorded for $\lambda_B = 488$ nm and $\lambda_Y = 590$ nm. $K_{g,1}$ and $K_{g,2}$ represent the grating vectors of the two multiplexed holograms for λ_B and λ_Y, respectively. The two probe wavelengths share the same incident axis. The separation between the two Bragg-matched diffracted beams is $\Delta\theta = 1.5$ deg.
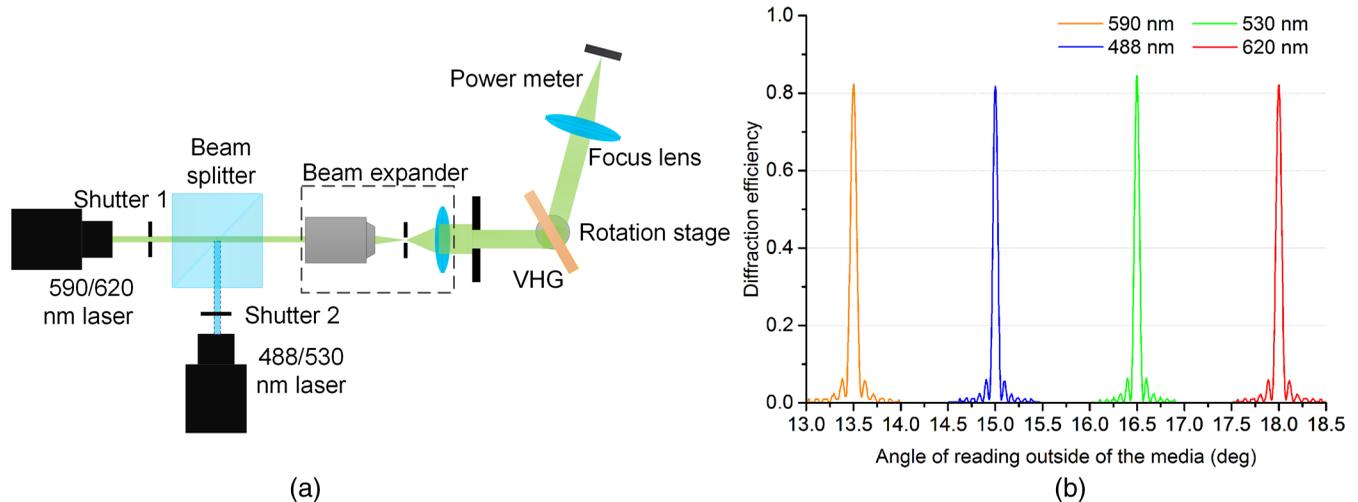
Fig. 2 (a) Experimental setup for measuring the spectral-angular selectivity at different target wavelengths. (b) The measured spectral-angular selectivity curves of the four multiplexed volume holograms. The diffraction intensity of each laser beam is measured sequentially by switching the shutter placed in front of the laser head. The results show that the Bragg-matched diffraction efficiency of each hologram is higher than 0.8.
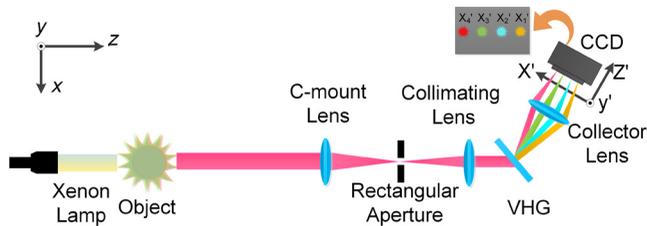
Fig. 3 Experimental setup of the simultaneous multispectral imaging system. The multiplexed VHG is placed on the Fourier plane of the 4*f* system combined with the collimating lens and the collector lens. Each hologram diffracts the Bragg-matched component of the incident beam. The collector lens projects laterally separated images formed with different wavelengths on the CCD camera.

the C-mount lens, the system can simultaneously acquire four multispectral images of the whole mouse. However, this is done by sacrificing the resolution of the whole system. The spectral-angular selectivity of the volume holograms can also affect the contrast of the images. When the imaging system is illuminated by a broadband point source, due to the spectral-angular selectivity of the volume hologram, the intensity of the point spreads along the transverse direction. The image intensity of each point is superimposed by a weighted intensity of its lateral neighbor points. The transverse features of ~1.58 mm can be resolved, while the contrast of the longitudinal features are severely affected.

An eight-week-old nude female mouse was anesthetized through intraperitoneal injection of 0.225 mL avertin solution and illuminated with the Xenon lamp. The multispectral images shown in Fig. 4(b) are simultaneously captured by the CCD detector without using bandpass filters. The image is rescaled

into an array with all entries in [0, 1], and the contrast is enhanced by setting the minimum threshold as 0.13. Because the spectral-angular selectivity of the 590 and 620 nm holograms is inferior to the 488 and 530 nm holograms, the intensity superposition in the 590 and 620 nm images appears more significant than that in the 488 and 530 nm images. Another factor that affects the intensity and contrast of the four images is that biological tissues have higher absorption coefficients for blue and green wavelengths.[15]

To verify the bandwidth of each single-band image, a white blank cardboard illuminated with Xenon lamp was placed $D = 35$ cm away from the objective lens. The relationship between the axial FOV_x and the bandwidth of illumination is given by[16]

$$\Delta\lambda_i = \frac{2\lambda_i f_{\text{col}}\text{FOV}_x}{f_{\text{obj}}\theta_{i,s}D}, \tag{3}$$

where $\Delta\lambda_i$ is the bandwidth of each single-band image, λ_i is the designated wavelength of each hologram, $\theta_{i,s}$ is the angle between the incident beam and the diffracted beam of each wavelength, f_{col} and f_{obj} are the focal lengths of the collimating lens and the C-mount lens, respectively. According to Eq. (3), the theoretical full-width-half-maximum (FWHM) bandwidths of the four single-band image are 25.24, 26.43, 26.77, and 28.79 nm, respectively. The measured FWHM bandwidths are 27.4, 23.4, 26.2, and 32.3 nm, respectively [Fig. 4(c)]. The deviations are mainly caused by the slight mechanical shifts of the spectrometer probe and the difference in the spectral-angularity selectivity of the four holograms. The central location x_i' of each Bragg-matched image on the detector plane can be calculated as
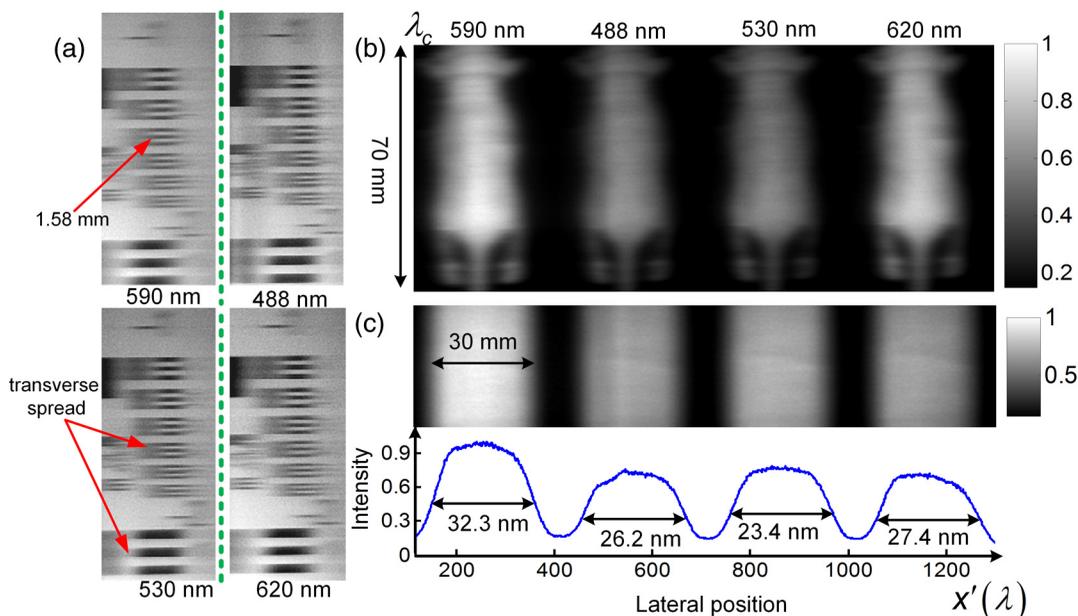
Fig. 4 (a) Resolution measurement of the simultaneous multispectral imaging system. Due to the intensity spread in the transverse direction, the image shows different contrast in the transverse and longitudinal direction. The transverse features of Group-1 Element 3 have 0.63 line pairs/mm and can be resolved, while the longitudinal features of Element 1 cannot be resolved due to the contrast degradation caused by the transverse spread of intensity. (b) Four single-band images of the nude mouse are simultaneously obtained with reflection-mode illumination. (c) The FOV_x and corresponding bandwidth of each single-band image are measured with the white blank cardboard.

$$x'_{i,c} = f_{col}(\theta_{i,dif} - \theta_{1,dif}),\qquad(4)$$

where f_{col} is the focal length of the collector lens and $\theta_{i,dif}$ is the diffraction angle of the i'th wavelength.

The mouse then underwent *in vivo* fluorescence imaging. All *in vivo* procedures were carried out under the protocol approved by the Ethical Committee of Tsinghua University. Two fluorescent beads (diameter 3 mm and length 7 mm) filled with two kinds of 1.0 mg/mL Qdots solutions (Qdots 530 and Qdots 620) were buried subcutaneously (∼0.6 mm) into two sites separately, i.e., the right upper abdomen and the left lower abdomen, as shown in Fig. 5(a). To avoid the movement of fluorescent beads caused by respiration, a colorless transparent acrylic sheet with a thickness of 2 mm and a width of 30 mm was used to fix the mouse on the sample holder. Then, the two beads were excited with a narrow-band light source of 480 nm. An emission long-pass filter of 500 nm was used to block the excitation light during the fluorescence imaging procedure. Figures 5(b) and 5(c) are the images of Qdots 620 and Qdots 530 fluorescent beads, respectively. The image of the blue channel shown in Fig. 5(d) is obtained by removing the emission long-pass filter.

The *in vivo* experimental results indicate that the multispectral fluorescence imaging system using multiplexed VHG can simultaneously obtain both spectral and positional information of the fluorescence emitted from the mouse in one shot. The imaging depth can be improved by increasing the intensity of excitation light. However, because both the excitation and emission wavelengths used in this system are within visible band, it is a challenge for this system to image fluorescence objects at depths beyond a couple of millimeters.

In summary, a simultaneous multispectral imaging system constructed with few optical components (i.e., only four components) was proposed. The system can provide complementary information of both fluorescence distribution and nonfluorescence profile of biological tissues. The multiplexed VHG in the imaging system selectively diffracts the desired wavelengths emitted or scattered from the object, with each being imaged

simultaneously on the detector plane and laterally separated from one another. Since each hologram for the specific target wavelength can be superimposed within the volume with the same recording wavelength, the use of spectrally multiplexed VHG as a spectroscopic device can provide more flexibility in deciding the number and the combination of target spectral bands of the multiplexed holograms to meet different multispectral imaging requirements. Although the diffraction efficiencies can be affected by the multiplexing procedure, the VHG can still keep high diffraction efficiency when the number of multiplexed holograms is within the capacity of the recording materials.[17]

References

1. M. S. Kim et al., "Steady-state multispectral fluorescence imaging system for plant leaves," *Appl. Opt.* **40**(1), 157–166 (2001).
2. D. Roblyer et al., "Multispectral optical imaging device for in vivo detection of oral neoplasia," *J. Biomed. Opt.* **13**(2), 024019 (2008).
3. M. E. Martin et al., "Development of an advanced hyperspectral imaging (hsi) system with applications for cancer detection," *Ann. Biomed. Eng.* **34**(6), 1061–1068 (2006).
4. Z. Nie et al., "Hyperspectral fluorescence lifetime imaging for optical biopsy," *J. Biomed. Opt.* **18**(9), 096001 (2013).
5. S. K. Shriyan et al., "Electro-optic polymer liquid crystal thin films for hyperspectral imaging," *J. Appl. Remote Sens.* **6**(1), 063549 (2012).
6. J. Downing and A. R. Harvey, "Multi-aperture hyperspectral imaging," in *Imaging and Applied Optics*, OSA Technical Digest, paper JW2B. 2, Optical Society of America (2013).
7. L. Gao, R. T. Kester, and T. S. Tkaczyk, "Compact image slicing spectrometer (iss) for hyperspectral fluorescence microscopy," *Opt. Express* **17**(15), 12293–12308 (2009).
8. B. K. Ford et al., "Computed tomography-based spectral imaging for fluorescence microscopy," *Biophys. J.* **80**(2), 986–993 (2001).
9. E. M. Winter, "Methods for determining best multispectral bands using hyperspectral data," in *2007 IEEE Aerospace Conf.*, pp. 1–6, IEEE (2007).
10. Y. Luo, S. B. Oh, and G. Barbastathis, "Wavelength-coded multifocal microscopy," *Opt. Lett.* **35**(5), 781–783 (2010).
11. Y. Luo et al., "Laser-induced fluorescence imaging of subsurface tissue structures with a volume holographic spatial-spectral imaging system," *Opt. Lett.* **33**(18), 2098–2100 (2008).
12. L. Cao et al., "Imaging spectral device based on multiple volume holographic gratings," *Opt. Eng.* **43**(9), 2009–2016 (2004).
13. L. Yuan et al., "Simulations and experiments of aperiodic and multiplexed gratings in volume holographic imaging systems.," *Opt. Express* **18**(18), 18839–19285 (2010).
14. A. Sinha and G. Barbastathis, "Broadband volume holographic imaging," *Appl. Opt.* **43**(27), 5214–5221 (2004).
15. S. L. Jacques, "Optical properties of biological tissues: a review.," *Phys. Med. Biol.* **58**(11), R37–R61 (2013).
16. A. Sinha and G. Barbastathis, "Broadband volume holographic imaging," *Appl. Opt.* **43**(27), 5214–5221 (2004).
17. X. Liu et al., "Optimization of a thick polyvinyl alcohol-acrylamide photopolymer for data storage using a combination of angular and peristrophic holographic multiplexing," *Appl. Opt.* **45**(29), 7661–7666 (2006).

Fig. 5 Simultaneous *in vivo* fluorescence imaging experiments. (a) The nude mouse with two subcutaneously buried fluorescent beads photographed with a conventional camera. (b) and (c) are the simultaneously acquired fluorescence images of Qdots 620 and Qdots 530 fluorescent beads with the proposed imaging system, respectively. (d) The blue channel image obtained without the emission longpass filter. Complementary information of the mouse can be visualized in (e), which was obtained by overlaying fluorescence images on the blue channel image.